FISEVIER

Contents lists available at ScienceDirect

Microporous and Mesoporous Materials

journal homepage: www.elsevier.com/locate/micromeso



Synthesis of hierarchical lamellar MFI zeolites with sequential intergrowth influenced by synthetic gel composition



Laleh Emdadi^{a,b}, Dat T. Tran^b, Emily Schulman^a, Lu Wei^{a,c}, Wenjin Shang^d, Huiyong Chen^d, Dongxia Liu^{a,*}

- ^a Department of Chemical and Biomolecular Engineering, University of Maryland, College Park, MD, 20742, USA
- ^b U.S. Army Research Laboratory, RDRL-SED-E, 2800 Powder Mill Road, Adelphi, MD, 20783, USA
- ^c College of Materials Science and Engineering, Beijing University of Technology, Beijing, 100124, PR China
- ^d School of Chemical Engineering, Northwest University, Xi'an, Shaanxi, 710069, PR China

ARTICLE INFO

Keywords: Hierarchical zeolite Intergrowth 2D zeolite Mesoporosity Acid site accessibility

ABSTRACT

Hierarchical lamellar zeolites, comprised of both micro- and mesoporosity, afford high active site accessibility and mass transport in processing of bulky molecules. Here, we report the synthesis of hierarchical lamellar MFI zeolites with sequential intergrowth that is induced by composition variation in the standard recipe of $100SiO_2/0.5Al_2O_3/3C_{22.6-6}/18.5Na_2O/4000H_2O$, where $C_{22.6-6}$ stands for the diquaternary ammonium surfactant ($[C_{22}H_{45}-N^+(CH_3)_2-C_6H_{12}-N^+(CH_3)_2-C_6H_{13}]Br_2^-$) template. The influences of $C_{22.6-6}$ concentration, alkalinity, and aluminum amount on the intergrowth of hierarchical lamellar MFI zeolites were investigated. The consequences of intergrowth on mesoporosity were analyzed. In all studied synthesis conditions except for very low alkalinity, hierarchical lamellar MFI zeolites were successfully crystallized. The increasing template concentration in the synthesis gel resulted in an increase in intergrowth and thus mesoporosity in the hierarchical MFI products. The increasing alkalinity led to an increase and then a decrease in mesoporosity in the hierarchical MFI products, which reflects the same trend in intergrowth in the hydrothermal synthesis process. The aluminum concentration, however, did not significantly affect the intergrowth and mesoporosity of the resultant hierarchical MFI zeolites. The sequential intergrowth achieved by simple variation in the synthesis composition for lamellar MFI zeolites resulted in higher structure hierarchy, mesoporosity, and acid site accessibility in one-step.

1. Introduction

Zeolites are crystalline aluminosilicates of various structure types, pore connectivity, and framework compositions with typical pore sizes less than 2 nm [1–3]. They are widely used for adsorption, separation, and catalysis in chemical and petrochemical industry [4–6]. The processing of heavy feedstocks in these applications over the traditional three-dimensional (3D) microporous zeolites, however, is potentially limited by the active site accessibility and mass transport [1,3,7,8]. Significant research efforts have been made in the past decade to prepare hierarchical meso-/microporous zeolites that combine the intrinsic properties of micropores with the characteristics of fast mass transport and easy active site accessibility of mesopores to improve the zeolite performance in these applications [9–15].

Different methods have been reported for synthesis of hierarchical meso-/microporous zeolites [4,16–18], including templated synthesis [9,19,20], demetallization (desilication or dealumination) of 3D

microporous zeolites [21,22], and post-modification of two-dimensional (2D) lamellar zeolite precursors. As a relatively new type of zeolite, 2D lamellar zeolite precursor contains stacked sheets of one-to-two unit cell or smaller thickness that are linked by weak van der Waals force or hydrogen bonds. The weak interlayer interactions in 2D zeolite precursors determine a variety of structural and chemical modifications can be potentially made in the gallery of adjacent zeolitic layers, with preservation of the original layer integrity. Therefore, 2D zeolite precursors can be post-modified via intercalation, exfoliation, pillaring, etc., to make pillared and delaminated zeolites with hierarchical microand mesoporous structures [23,24]. It should be noted that this synthesis approach often involves multiple steps. A single-step synthesis of 2D zeolites with pillared and/or delaminated structures to increase mesoporosity and structure hierarchy is desired from the process economy point of view.

The multi-lamellar MFI, a zeolite consisting of several layers of 2D MFI nanosheets, has been the most recently reported 2D zeolite

E-mail address: liud@umd.edu (D. Liu).

^{*} Corresponding author.

precursor [23-25]. The synthesis of multi-lamellar MFI was achieved via a hydrothermal crystallization of the synthesis gel comprising of tetraethyl orthosilicate (TEOS) (or sodium silicate ((Na₂SiO₂)_nO)), aluminium sulphate (Al₂(SO₄)₃), sodium hydroxide (NaOH), sulfuric acid (H₂SO₄), distilled water, and C₂₂₋₆₋₆ template with a molar com $position \quad of \quad 100 SiO_2/10C_{22\text{-}6\text{-}6}/30 Na_2O/1Al_2O_3/18H_2SO_4/4000H_2O.$ The C₂₂₋₆₋₆ template is a diquaternary ammonium surfactant with a chemical structure of $[C_{22}H_{45}-N^+(CH_3)_2-C_6H_{12}-N^+(CH_3)_2-C_6H_{13}]$ Br₂, in which the diquaternary ammonium portion directs the micropore formation within each zeolitic layer and the hydrocarbon tail serves as a space-filler between the zeolitic layers to create the lamellar structure [24,26]. The effects of composition variation in the synthesis recipe on the resultant 2D multi-lamellar MFI zeolites were studied by varying the head group structures and/or alkyl chain lengths in the templates [27], the type of template counterions [28], the Na+ concentration [24,25,29], crystallization under static condition [30], etc. It has been shown that the increase in the number of ammonium groups in the template increased the nanosheet thickness. The replacement of the Br^{-} ion in the template by $HC_2O_4^{-}$, $C_2O_4^{2-}$, CO_3^{2-} , $H_2PO_4^{-}$, HPO_4^{2-} , etc. led to formation of amorphous material or micron-sized MFI spheres comprised of flat or wave-like nanosheet aggregates. The Na ions took part in the structure directing process to increase the nanosheet thickness upon its generation under the assistance of surfactant template. The hydrothermal synthesis under static condition, in contrast to the rotation condition [24,25,27], also led to success in crystallization of 2D multi-lamellar MFI zeolite. As indicated above, all these studies were based on the modulation of 100SiO₂/10C₂₂₋₆₋₆/ $30Na_2O/1Al_2O_3/18H_2SO_4/4000H_2O$.

Here, we report the synthesis of mutli-lamellar MFI zeolite using a simple composition of $100 SiO_2/3C_{22-6-6}/10 Na_2O/1Al_2O_3/4000H_2O$. In comparison to previously reported synthesis composition [12,25], the usage of C_{22-6-6} template was significantly reduced and sulfate salt was eliminated. The effects of C22-6-6 concentration, alkalinity, and aluminum amount in the synthetic gel on the structure and morphology of resultant multi-lamellar MFI zeolites were studied. With increasing C22-6-6 template in the synthesis composition, the mesoporosity of the resultant 2D lamellar MFI was increased. The alkalinity of the zeolite synthetic gel was increased by increasing the quantity of Na2O (i.e., NaOH) in the composition, which resulted in an increase and then decrease in mesoporosity in the final products. The aluminum content did not obviously influence the textural properties of the obtained 2D lamellar MFI zeolites. A further analysis on the structure of 2D lamellar MFI zeolites indicated the presence of sequential intergrowth among zeolite nanosheets. The intergrowth led to the formation of hierarchical lamellar MFI with improved mesoporosity, acid site accessibility, and structure hierarchy that can be simply tuned by variation in the synthesis composition in one-step.

2. Experimental

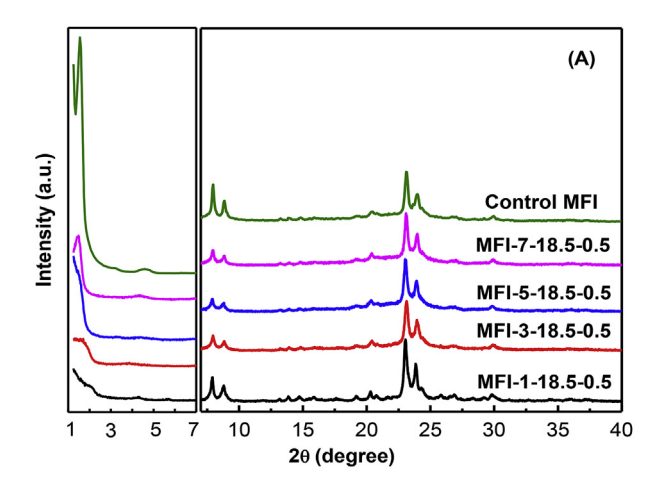
2.1. Materials

Aluminum isopropoxide (metal basis) (Al [OCH(CH₃)₂]₃, 99.99+% purity) and isopropylamine ((CH₃)₂CHNH₂, > 99%) were purchased from Alfa Aesar. Tetraethyl orthosilicate (TEOS, 98%), sodium hydroxide (NaOH, \geq 97.0%), methanol (CH₃OH, > 99%), and ammonium nitrate (NH₄NO₃, \geq 99.0%) were supplied by Sigma-Aldrich. Deionized (DI) water was used throughout the experiment. 2,6-di-*tert*-butylpyridine (DTBP, > 97%) was purchased from TCI America. Diquaternary ammonium surfactant ([C₂₂H₄₅-N⁺(CH₃)₂-C₆H₁₂-N⁺(CH₃)₂-C₆H₁₃] Br₂, (C₂₂₋₆₋₆)) was synthesized based on the method reported by Ryoo et al. [25] and the C₂₂₋₆₋₆ synthesis method has also been described in our previous publications [31,32].

Table 1Composition for crystallization of the hierarchical lamellar MFI zeolite samples.

Zeolite sample	Composition in molar ratios ^a				
	SiO ₂	C ₂₂₋₆₋₆ (x)	Na ₂ O (y)	Al ₂ O ₃ (z)	H ₂ O
MFI-1-18.5-0.5	100	1	18.5	0.5	4000
MFI-3-18.5-0.5	100	3	18.5	0.5	4000
MFI-5-18.5-0.5	100	5	18.5	0.5	4000
MFI-7-18.5-0.5	100	7	18.5	0.5	4000
MFI-3-15-0.5	100	3	15	0.5	4000
MFI-3-10-0.5	100	3	10	0.5	4000
MFI-3-5-0.5	100	3	5	0.5	4000
MFI-3-0.5-0.5	100	3	0.5	0.5	4000
MFI-3-10-0.67	100	3	10	0.67	4000
MFI-3-10-1.0	100	3	10	1	4000
MFI-3-10-2.0	100	3	10	2	4000

^a The general recipe is $100SiO_2/xC_{22-6-6}/yNa_2O/zAl_2O_3/4000H_2O$.



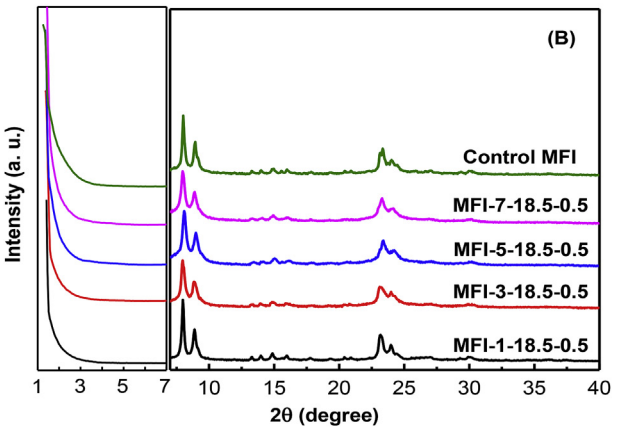


Fig. 1. Low-angle and wide-angle XRD patterns of the synthesized MFI-1-18.5-0.5, MFI-3-18.5-0.5, MFI-5-18.5-0.5, and MFI-7-18.5-0.5 zeolite samples, before (A) and after (B) template removal by calcination, respectively. Control MFI has also been shown in (A) and (B) for comparison purpose.

2.2. Synthesis of hierarchical lamellar MFI zeolite

The molar composition of $100 \mathrm{SiO}_2/3 C_{22-6-6}/18.5 \mathrm{Na}_2 \mathrm{O}/0.5 \mathrm{Al}_2 \mathrm{O}_3/4000 \mathrm{H}_2 \mathrm{O}$ was used as the standard recipe to synthesize the hierarchical multi-lamellar MFI zeolite. To further our understanding of effects of surfactant template, alkalinity, and Si/Al ratio in the synthesis, we conducted a series of experiments to investigate the influence of these experimental parameters on the multi-lamellar MFI formation. Table 1 summarizes all the compositions we have tested in our study. Individual experimental variables (x: C_{22-6-6} concentration, y: Na_2O concentration,

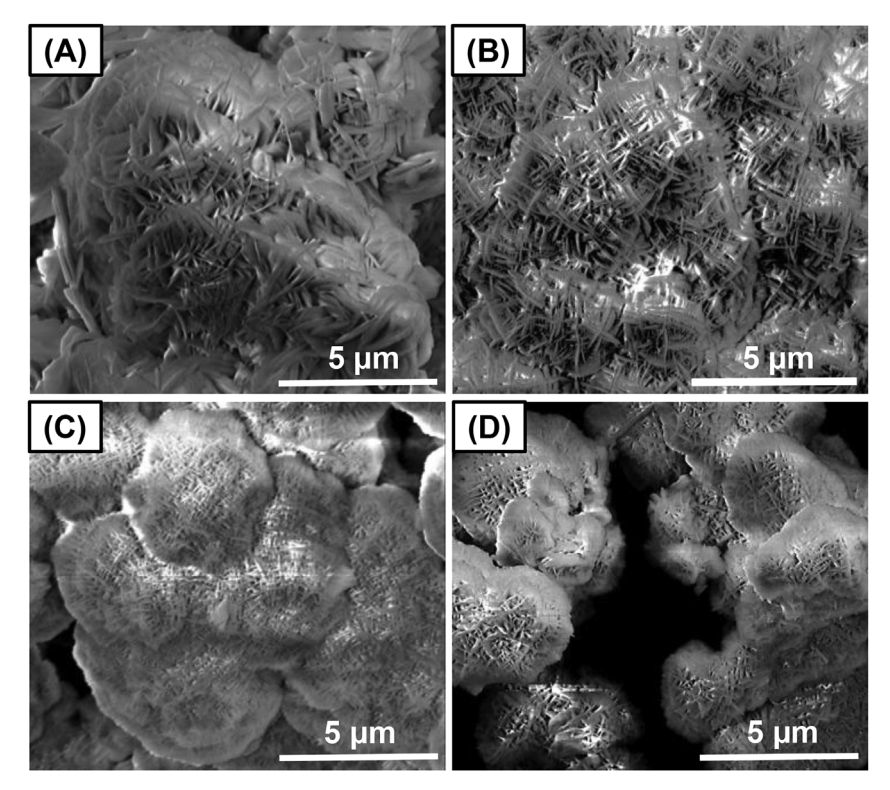
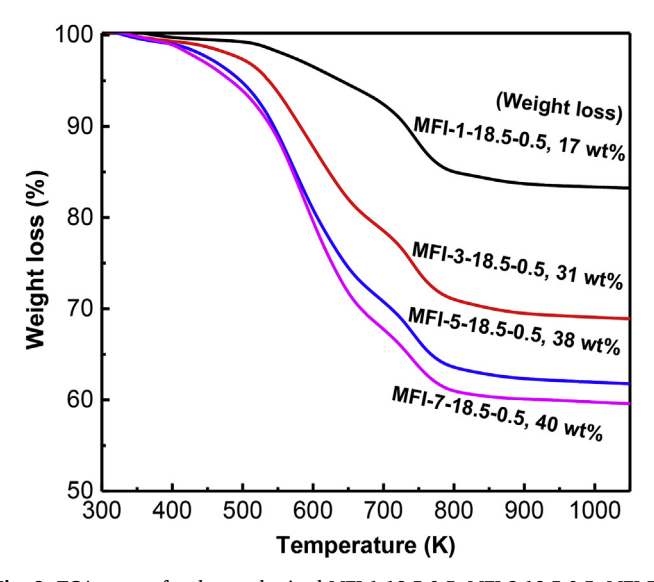


Fig. 2. SEM images of the synthesized MFI-1-18.5-0.5 (A), MFI-3-18.5-0.5 (B), MFI-5-18.5-0.5 (C), and MFI-7-18.5-0.5 (D) zeolite samples, respectively.



 $\begin{tabular}{ll} Fig. 3. TGA curves for the synthesized MFI-1-18.5-0.5, MFI-3-18.5-0.5, MFI-3-18.5-0.5, and MFI-7-18.5-0.5 zeolite samples, respectively. \\ \end{tabular}$

and z: Al₂O₃ concentration) were changed, and the effects of changing these variables (C₂₂₋₆₋₆ template (x), alkalinity (y), and aluminum amount (z), respectively) were investigated by comparing the product to that obtained with the standard synthesis recipe.

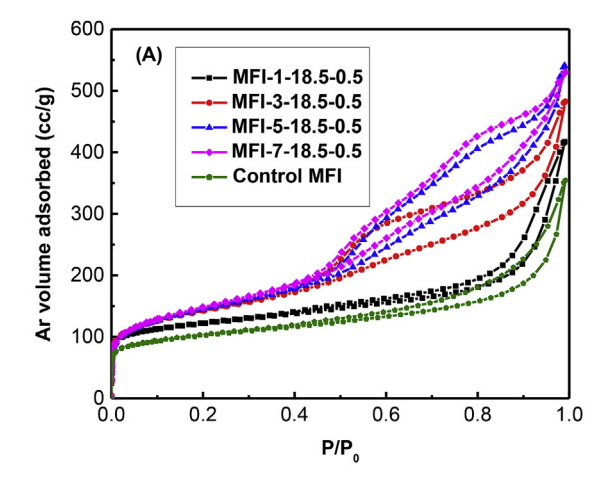
In the typical synthesis process, 0.41 g NaOH was dissolved in 11.5 g DI water, followed by dissolution of 0.06 g of Al [OCH(CH₃)₂]₃ in this solution using sonication at room temperature for 0.5 h. Afterwards, 5.78 g TEOS was added, and the resultant mixture was stirred vigorously at room temperature for 8 h. The C₂₂₋₆₋₆ solution that was prepared by dissolving the desired amount in 8.5 g of DI water at 333 K was then added into the above mixture. The resultant zeolite synthesis gel was continuously stirred at room temperature for 2 h before transferring it into a Teflon-lined stainless-steel autoclave. Finally,

crystallization of zeolite was conducted for 5 days in the autoclaves tumbling vertically in an oven heated at 423 K. After crystallization, the zeolite sample was filtered, washed with DI water till pH \sim 9, and dried at 343 K overnight. The as-obtained zeolite samples were named on the basis of x, y, and z values used in the synthesis composition, as shown in Table 1. For example, MFI-1-18.5-0.5 denotes the composition of $100\text{SiO}_2/1\text{C}_{22-6-6}/18.5\text{Na}_2\text{O}/0.5\text{Al}_2\text{O}_3/4000\text{H}_2\text{O}}$ in the synthesis composition. For comparison, the multi-lamellar MFI, named control MFI, was prepared using the molar composition of $100\text{SiO}_2/10\text{C}_{22-6-6}/30\text{Na}_2\text{O}/1\text{Al}_2\text{O}_3/18\text{H}_2\text{SO}_4/4000\text{H}_2\text{O}}$, according to the procedure reported by Ryoo et al. [25].

The as-synthesized MFI zeolites were then calcined at 873 K for 6 h in flowing air (1.67 mL s $^{-1}$, ultrapure air, Airgas) after heating the sample from room temperature (298 K) to 873 K using ramping rate of 0.0266 K s $^{-1}$. After this, the MFI zeolite samples were ion-exchanged three times using 1 M aqueous NH₄NO₃ (weight ratio of zeolite to NH₄NO₃ solution = 1:10) at 353 K for 12 h, and subsequently, collected by centrifugation, washed with deionized water three times (weight ratio of zeolite to water = 1:10), and dried at 343 K overnight. All zeolite samples in their NH₄ $^+$ -form were treated in dry air (1.67 mL s $^{-1}$, ultrapure, Airgas) by increasing the temperature from ambient temperature to 823 K at 0.0242 K s $^{-1}$ and holding for 4 h to thermally decompose NH₄ $^+$ to NH₃ and H $^+$.

2.3. Product characterization

Scanning electron microscopy (SEM) and transmission electron microscopy (TEM) images of the hierarchical lamellar MFI zeolites were recorded on a FEI Quanta 200 F scanning electron microscope and a JEM 2100 LaB6 transmission electron microscope, respectively. Powder X-Ray diffraction (XRD) patterns were collected using a Rigaku Ultima III diffractometer (CuK_{α} radiation) in the 20 range from 1 to 40° with a scan rate of 1° per minute. The Ar sorption isotherms were measured using an Autosorb-iQ analyzer (Quantachrome Instruments) at 87 K. Prior to the measurement, sample was evacuated overnight at 623 K and 1 mm Hg. The thermogravimetric analysis (TGA) was performed in



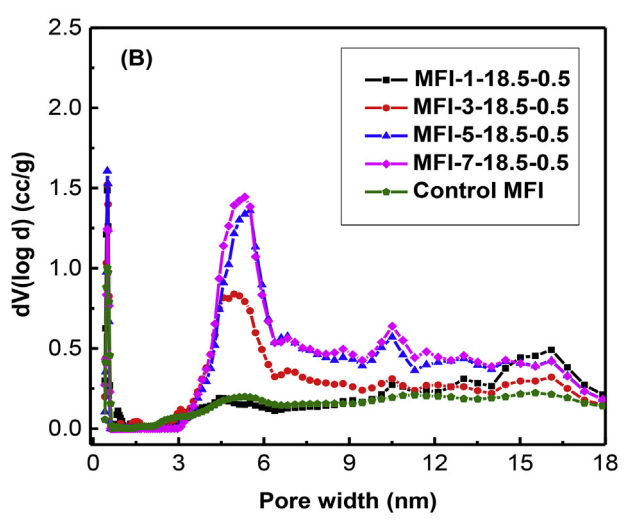
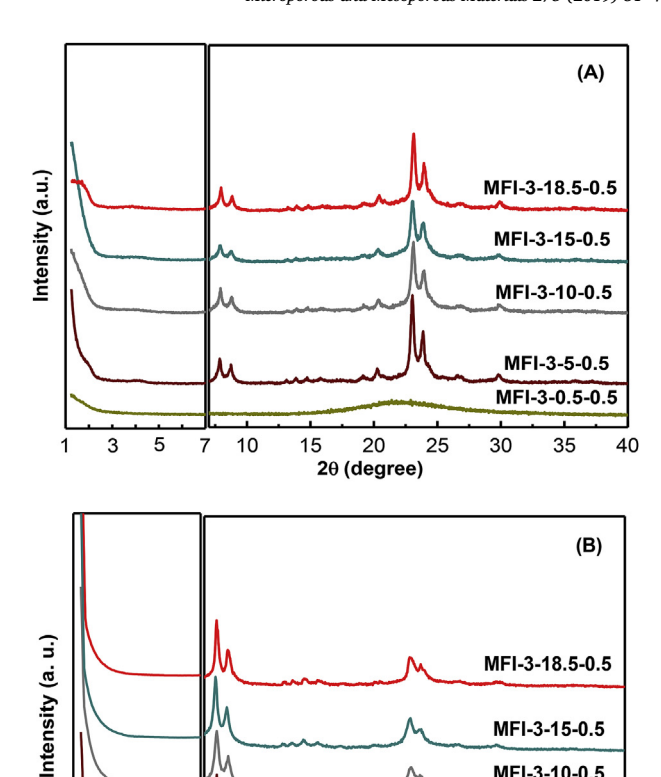


Fig. 4. Ar adsorption-desorption isotherms (A) and NLDFT pore size distributions (B) extracted from adsorption branch of the Ar isotherms for MFI-1-18.5-0.5, MFI-3-18.5-0.5, MFI-3-18.5-0.5, and MFI-7-18.5-0.5 zeolite samples, respectively. Control MFI has also been shown here for comparison purpose.

a TGA instrument (PerkinElmer TGA 7 thermogravimetric analyzer) from 303 K to 1050 K under air flow of 1.667 mL s $^{-1}$ with a heating rate of 0.167 K s $^{-1}$. The Si and Al contents of zeolite samples were determined by inductively coupled plasma optical emission spectroscopy (ICP-OES, Perkin Elmer Optima 7000).

The concentration of Brønsted acid sites in each hierarchical zeolite sample was quantified by the reactive gas chromatography (RGC) method using isopropylamine ($CH_3CH(NH_2)CH_3$) as the probe molecule, following the report from Abdelrahman et al. [33]. The selective decomposition of isopropylamine adsorbate on Brønsted acid site



MFI-3-10-0.5

MFI-3-5-0.5

MFI-3-0.5-0.5

MFI-3-0.5-0.5

MFI-3-0.5-0.5

MFI-3-0.5-0.5

MFI-3-0.5-0.5

MFI-3-0.5-0.5

Fig. 5. Low-angle and wide-angle XRD patterns of the synthesized MFI-3-0.5-0.5, MFI-3-5-0.5, MFI-3-10-0.5, MFI-3-15-0.5, and MFI-3-18.5-0.5 zeolite samples before (A) and after (B) template removal by calcination, respectively.

 $(CH_3CH(NH_2)CH_3\cdots AlO(H)Si)$ in zeolites via Hoffmann elimination forms propylene and ammonia. The quantification of propylene by a gas chromatograph (GC) instrument determined the number of Brønsted acid (AlO(H)Si) sites in each zeolite sample. The acid site accessibility was evaluated by methanol (CH_3OH) dehydration to dimethyl ether (DME) in the presence of 2,6-di-tert butylpyridine (DTBP) organic base at differential conversions (< 2%) at 433 K. Liquid mixture of methanol (Sigma-Aldrich, > 99%) and DTBP (TCI America, > 97% purity) was introduced into a flowing He stream using a syringe pump (NE 1000, New Era Pump System Inc.). The reactor effluent was sent via heated transfer lines to a mass spectrometer (MS, Ametek Proline). The methanol dehydration rate was measured as DTBP titrant was continuously added until it reached a plateau. The loss in methanol reaction rate reflects the degree of accessibility of bulky DTBP

Table 2Textural properties of the MFI-x-18.5-0.5 samples determined from Ar isotherms.

Zeolite sample	$V_{micro}^{a} [cm^3g^{-1}]$	$S_{micro}^{a} [m^2 g^{-1}]$	$S_{ext}^{a} [m^2 g^{-1}]$	V _t ^b [cm ³ g ⁻¹]	V _{meso} ^c [cm ³ g ⁻¹]	S_{BET}^{d} [m ² g ⁻¹]
MFI-1-18.5-0.5	0.068	188	206	0.591	0.523	394
MFI-3-18.5-0.5	0.060	141	304	0.652	0.592	445
MFI-5-18.5-0.5	0.057	132	397	0.689	0.632	529
MFI-7-18.5-0.5	0.050	123	446	0.697	0.647	569
Control MFI ^e	0.063	141	169	0.277	0.214	310

^a Determined from t-plot method.

^b Determined by NLDFT method.

^c Determined from $V_{meso} = V_t - V_{micro}$.

^d Determined from Brunauer, Emmett, and Teller (BET) method.

e Control MFI has also been shown here for comparison purpose.

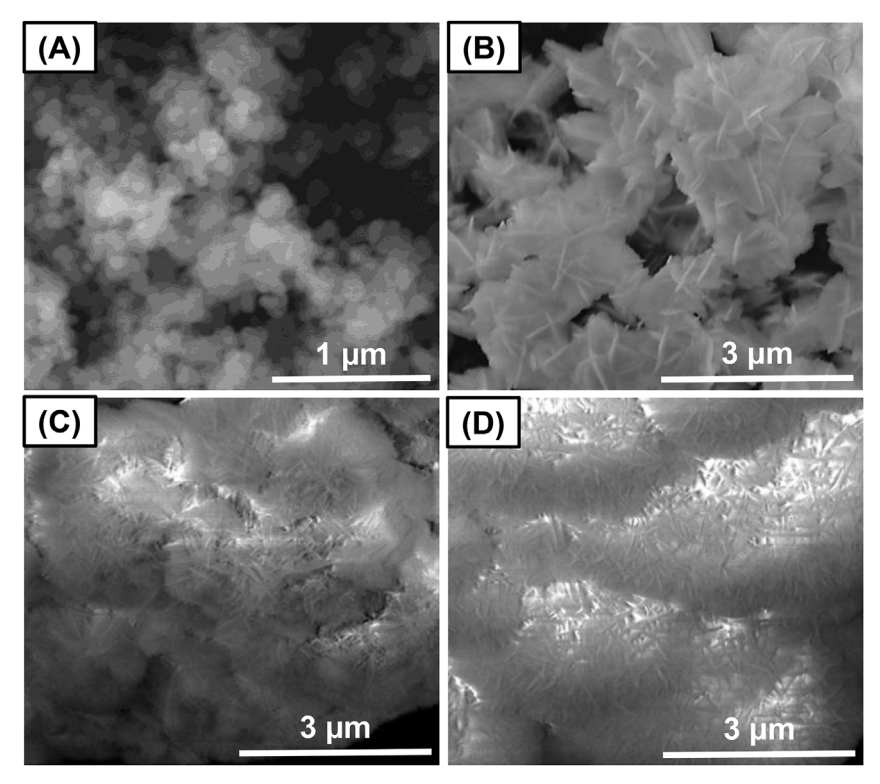


Fig. 6. SEM images of the synthesized MFI-3-0.5-0.5 (A), MFI-3-5-0.5 (B), MFI-3-10-0.5 (C), and MFI-3-15-0.5 (D) zeolite samples, respectively.

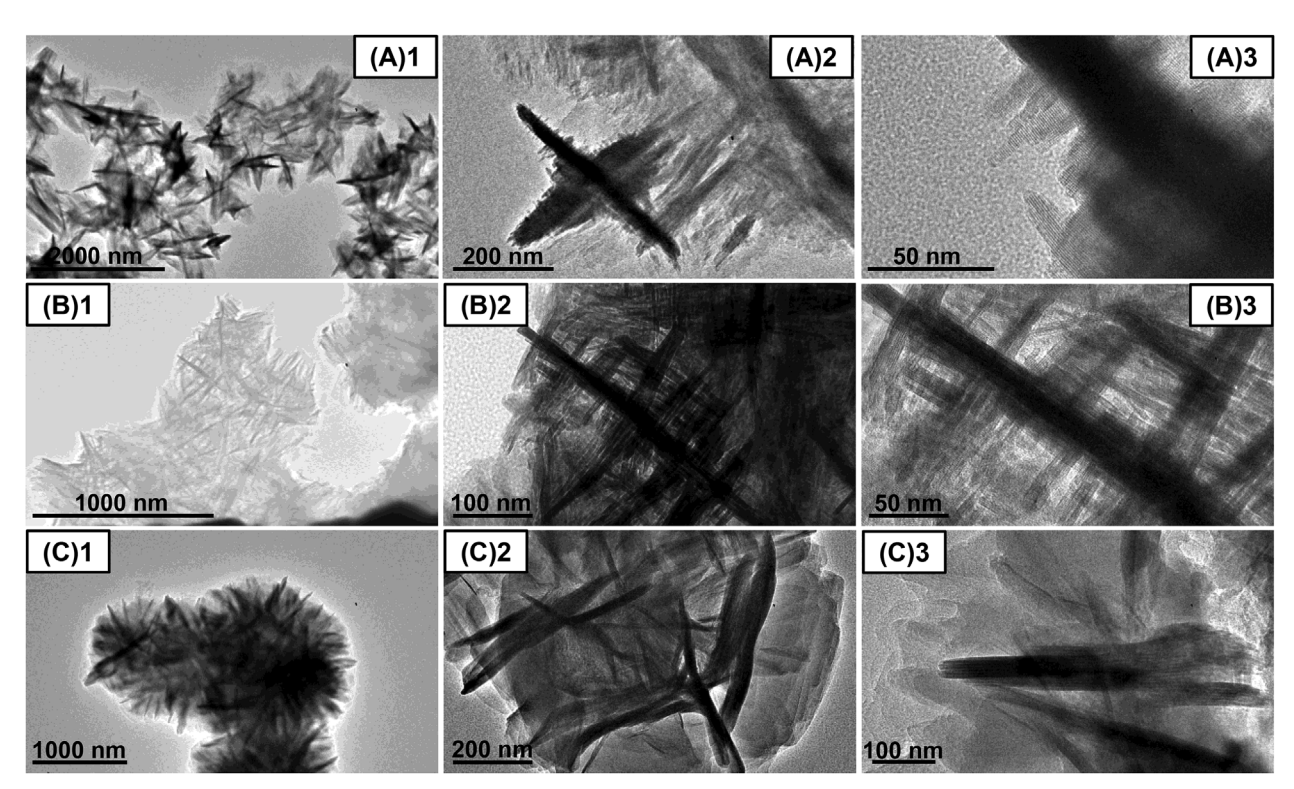


Fig. 7. TEM images of the synthesized MFI-3-5-0.5 (A)1-3, MFI-3-10-0.5 (B)1-3, and MFI-3-15-0.5 (C)1-3 zeolite samples, respectively.

molecules to Brønsted acid sites in zeolites, and hence, the fraction of external acid sites was defined as the degree of methanol reaction rate loss. Details of reaction set-up and method for external acid site determination have been described in our previous publications [34–36].

3. Results and discussion

3.1. Effect of C_{22-6-6} concentration on synthesis of hierarchical lamellar MFI realite

We firstly studied the effect of C_{22-6-6} template content on the resultant hierarchical lamellar MFI products by varying the C_{22-6-6}

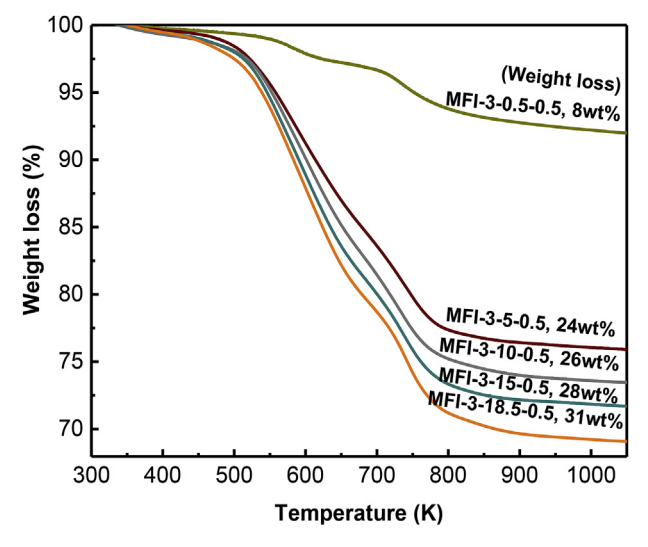
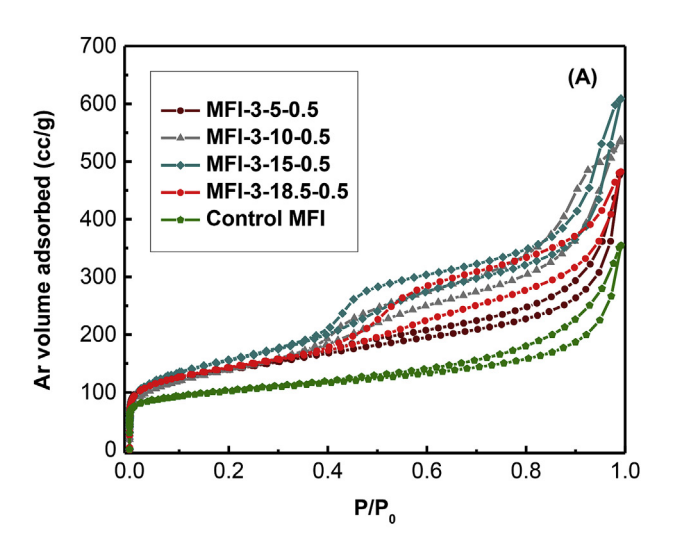


Fig. 8. TGA curves for the synthesized MFI-3-0.5-0.5, MFI-3-5-0.5, MFI-3-10-0.5, MFI-3-15-0.5, and MFI-3-18.5-0.5 zeolite samples, respectively.



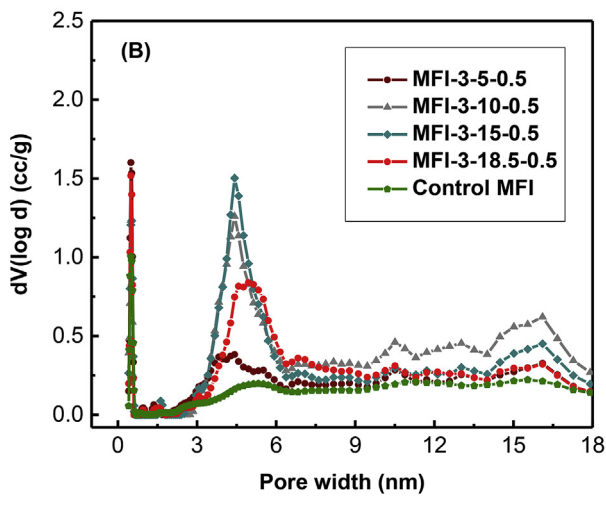


Fig. 9. Ar adsorption-desorption isotherms (A) and NLDFT pore size distribution (B) extracted from adsorption branch of the Ar isotherms for the synthesized MFI-3-5-0.5, MFI-3-10-0.5, MFI-3-15-0.5, and MFI-3-18.5-0.5 zeolite samples, respectively. Control MFI has also been shown here for comparison purpose.

concentration (x) from 1 to 3, 5, and 7, respectively, while keeping other components constant. Fig. 1(A) and (B) show the XRD patterns of the synthesized products (designated as MFI-1-18.5-0.5, MFI-3-18.5-0.5, MFI-5-18.5-0.5, and MFI-7-18.5-0.5) before and after template removal by calcination, respectively. The wide-angle XRD peaks in each spectrum in Fig. 1 are characteristics of the crystalline MFI zeolite structure, similar to what was observed for the synthesized control MFI [25]. This indicates that all these synthesis conditions, even at low C₂₂- $_{6-6}$ concentration (x = 1 for MFI-1-18.5-0.5), can fully crystallize MFI zeolite structure. The low-angle XRD peaks (represented by $2\theta = \sim 1.54^{\circ}$, for example) in Fig. 1(A) correspond to the first order reflection of the layered MFI precursor, which demonstrates the multilamellar structural feature of these samples after hydrothermal crystallization. The increase in the low-angle peak intensity with increasing the C₂₂₋₆₋₆ concentration from MFI-1-18.5-0.5 to MFI-7-18.5-0.5 shows that the long-range structural order of the multi-lamellar MFI zeolite increases [12]. The low-angle reflection peaks disappeared in the calcined hierarchical lamellar MFI samples, as shown in Fig. 1(B), which was caused by the collapses of zeolite layers upon organic surfactant template removal during the calcination process.

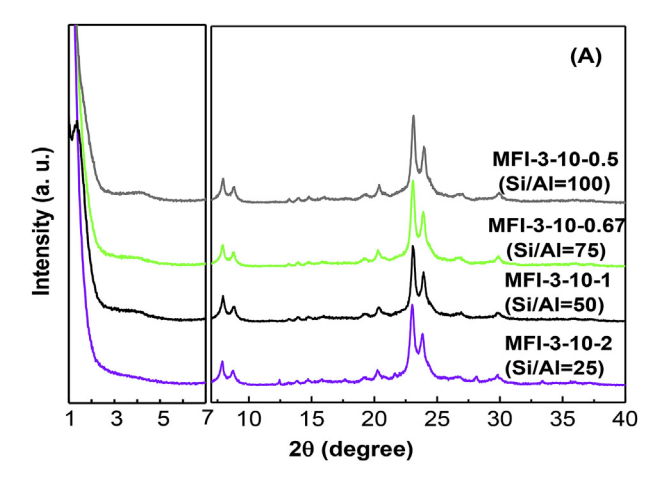
SEM was employed to provide detailed insights into the morphological changes of the synthesized hierarchical lamellar MFI zeolites with different C_{22-6-6} concentration in the synthesis gel. Fig. 2(A)-2(D) show the SEM images of MFI-1-18.5-0.5, MFI-3-18.5-0.5, MFI-5-18.5-0.5, and MFI-7-18.5-0.5, respectively, all of which contain plate-like structures stacked into porous spherical aggregates. MFI-1-18.5-0.5 consists of randomly organized multi-lamellar zeolite nanosheet stacks (Fig. 2(A)). By increasing the C₂₂₋₆₋₆ concentration in the synthesis recipe, the nanosheet stack arrangement changes to a more organized structure in MFI-3-18.5-0.5 (Fig. 2(B)) and finally a very organized house-of-cards like morphology for MFI-5-18.5-0.5 and MFI-7-18.5-0.5 in Fig. 2(C) and 2(D), respectively. The average thickness of the nanosheet stacks in MFI-1-18.5-0.5 is around 60 nm and changes by changing the C₂₂₋₆₋₆ concentration in the synthesis recipe. By increasing the C_{22-6-6} content, the plate-like structures tend to become thinner. This phenomenon can be explained by the cooperative structure directing effects of C22-6-6 and sodium ions (Na+) in the MFI growth process [29]. It is reported that MFI nanosheet is generated under the assistance of C₂₂₋₆₋₆ template, while the nanosheet thickness can be increased via growth directed by Na+ ions in the synthesis gel composition. The lower C₂₂₋₆₋₆ content, i.e., low C₂₂₋₆₋₆/Na⁺ ratio, induced the formation of less number of MFI nanosheets in the first place under the synthesis condition. Therefore, the silica and alumina sources in the synthetic gel tended to grow from the pre-formed MFI nanosheets under the templating effects of Na⁺ ions. As a result, thicker nanosheet stacks were formed in comparison with the ones with higher C_{22-6-6} content. In all cases, the intergrowth among zeolite plates occurred, which led to the porous window-like structure viewed from exterior of the resultant zeolite samples. The intergrowth of zeolite plate structures seems to increase with increasing C₂₂₋₆₋₆ content, which resulted in more ordered zeolite plate aggregates. Control MFI displayed the randomly organized structure, as shown in our previous work [31].

The involvement of $C_{22.6-6}$ as the zeolite template in formation of hierarchical lamellar MFI structures in the studied recipe was investigated by the TGA measurement of the as-synthesized samples. As shown in Fig. 3, the weight loss of hierarchical lamellar MFI particles increases from 17 wt% to 40 wt% with increasing the $C_{22.6-6}$ content in the zeolite synthesis compositions for MFI-1-18.5-0.5 to MFI-7-18.5-0.5 samples, respectively. The weight losses in MFI-5-18.5-0.5 and MFI-7-18.5-0.5 samples (38 wt% and 40 wt%, respectively) were similar to the one reported for control MFI in our previous publication (\sim 40%) [37]. Therefore, it can be concluded that the amount of $C_{22.6-6}$ used in the synthesis recipe for MFI-5-18.5-0.5 was already enough for production of well-organized multi-lamellar MFI zeolite structure. The additional $C_{22.6-6}$ used in MFI-7-18.5-0.5 and beyond might be helpful to maintain the zeolite long-range structural order, but seems not to be helpful to

Table 3Textural properties of the MFI-3-y-0.5 samples determined from Ar isotherms.

Zeolite sample	V_{micro}^{a} [cm 3 g $^{-1}$]	$S_{micro}^{a} [m^2 g^{-1}]$	$S_{ext}^{a} [m^2 g^{-1}]$	V_t^b [cm ³ g ⁻¹]	V_{meso}^{c} [cm 3 g $^{-1}$]	S_{BET}^{d} [m ² g ⁻¹]
MFI-3-5-0.5	0.058	163	275	0.630	0.572	437
MFI-3-10-0.5	0.056	118	340	0.700	0.644	458
MFI-3-15-0.5	0.054	107	415	0.785	0.731	521
MFI-3-18.5-0.5	0.060	141	304	0.652	0.592	445
Control MFI ^e	0.063	141	169	0.277	0.214	310

- ^a Determined from t-plot method.
- ^b Determined by NLDFT method.
- ^c Determined from $V_{meso} = V_t V_{micro}$
- ^d Determined from Brunauer, Emmett, and Teller (BET) method.
- ^e Control MFI has also been shown here for comparison purpose.



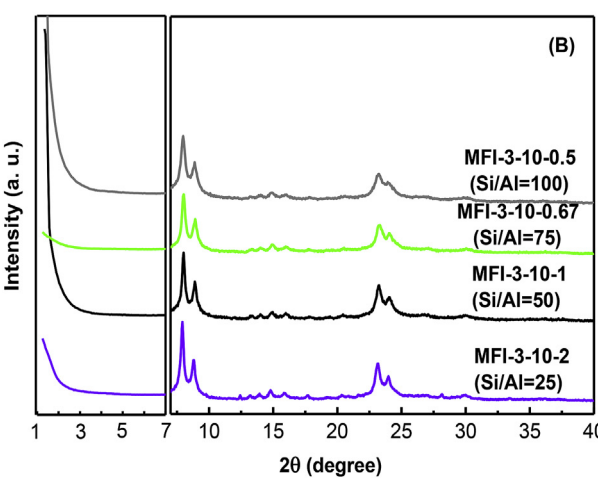


Fig. 10. Low-angle (A) and wide-angle (B) XRD patterns for the synthesized MFI-3-10-2 (Si/Al = 25), MFI-3-10-1 (Si/Al = 50), MFI-3-10-0.67 (Si/Al = 75), and MFI-3-10-0.5 (Si/Al = 100) before (A) and after (B) template removal by calcination.

template the growth of the hierarchical MFI zeolite materials.

The textural properties of hierarchical lamellar MFI zeolites synthesized with varying $C_{22\cdot 6\cdot 6}$ contents in the recipe were analyzed using Ar adsorption-desorption isotherms and the results are shown in Fig. 4. Fig. 4(A) illustrates that all these samples have type IV isotherm with hysteresis loops in relative pressure (P/P₀) range of 0.5–0.9 confirming their meso-/microporous structure [38,39]. Different shapes of the hysteresis loops in these samples indicate that they have different mesoporous or macroporous structures. For MFI-1-18.5-0.5 and control MFI, the hysteresis loop has H3 form that shows they have slit-shaped pores, while H4 type of hysteresis loop is observed in MFI-3-18.5-0.5, MFI-5-18.5-0.5, and MFI-7-18.5-0.5 samples, which demonstrates they

have narrower slit-shaped pores compared to the other two samples [38]. The non-local density functional theory (NLDFT) pore size distributions of these samples (Fig. 4(B)) determined from the adsorption branch of their isotherms illustrate that all these samples have microporous characteristic peaks of MFI (\sim 0.5 nm), but different mesopore size distributions. As it was expected, MFI-1-18.5-0.5 and control MFI have a broad pore size distribution compared to the other synthesized samples. The average size of the mesopores increases from 4.4 nm to 5.3 nm for MFI-1-18.5-0.5 and MFI-7-18.5-0.5 by adding more C_{22-6-6} in the synthesis recipe. Consistent with SEM observations, the increase in C_{22-6-6} template quantity in the synthesis led to higher number of nanosheets that consumed more silica and alumina sources in the synthetic gel. The intergrowth between zeolite nanosheets only occurred sparsely, which acted as pillars to keep the nanosheets apart while created the mesoporosity.

Table 2 summarizes the textural properties of the synthesized MFI samples with different concentrations of C_{22-6-6} in the recipe that were determined from the Ar isotherms. External surface area (Sext), mesopore volume (V_{meso}), total pore volume (V_t), and BET surface area (S_{BET}) of these zeolite samples increase by increasing the concentration of C₂₂₋₆₋₆ in the synthesis recipe due to the formation of more uniform mesopores with larger pore sizes. Micropore volume (V_{micro}) and micropore surface area (S_{micro}) decrease slightly by using more C_{22-6-6} in the synthesis recipe. This trend can be explained by generation of mesoporosity at the cost of partial loss in microporosity of the meso-/ microporous zeolites that has also been observed and reported by other researchers before [12,40,41]. The mesoporosity of all the synthesized samples is higher than the synthesized control MFI while their microporosity is comparable. The resultant MFI products showed a maximum BET surface area $(529-569 \text{ m}^2 \text{ g}^{-1})$ around $x = 5-7 \text{ C}_{22-6-6}$ in the synthesis recipe. The total pore volume also reached a maximum $(0.689-0.697 \text{ cm}^3 \text{ g}^{-1})$ in this range. The high surface area and total pore volume could be due to the intergrowth between the zeolite nanosheets, as discussed above.

3.2. Effect of alkalinity on synthesis of hierarchical lamellar MFI zeolite

Alkalinity is an important factor that influences the solubility of zeolite precursor, zeolite growth kinetics, product morphology, and zeolite textural properties [42–44]. Here, we studied the effects of zeolite synthesis gel alkalinity on morphology and textural properties of the resulted hierarchical lamellar MFI zeolites. Again, MFI-3-18.5-0.5 is our standard composition. The pH of the synthesis gel was varied by decreasing the Na₂O molar concentration (y) from 18.5 in MFI-3-18.5-0.5 sample to 15, 10, 5, and 0.5, respectively (Table 1).

Fig. 5 shows the XRD patterns of the as-obtained zeolites (designated as MFI-3-0.5-0.5, MFI-3-5-0.5, MFI-3-10-0.5, MFI-3-15-0.5, and MFI-3-18.5-0.5) before (Fig. 5(A)) and after (Fig. 5(B)) template removal by calcination, respectively. As shown in Fig. 5(A), when the concentration of Na_2O was very low (MFI-3-0.5-0.5), no crystalline zeolite phase was formed. By increasing the Na_2O concentration as

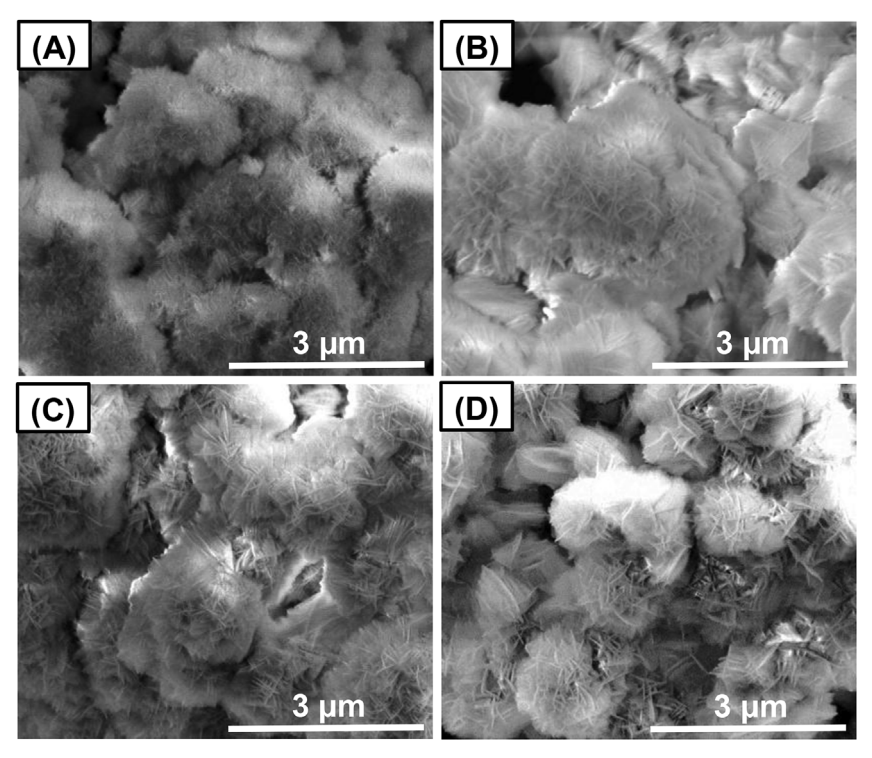


Fig. 11. SEM images of the synthesized MFI-3-10-2 (Si/Al = 25) (A), MFI-3-10-1 (Si/Al = 50) (B), MFI-3-10-0.67 (Si/Al = 75) (C), and MFI-3-10-0.5 (Si/Al = 100) (D) zeolite samples, respectively.

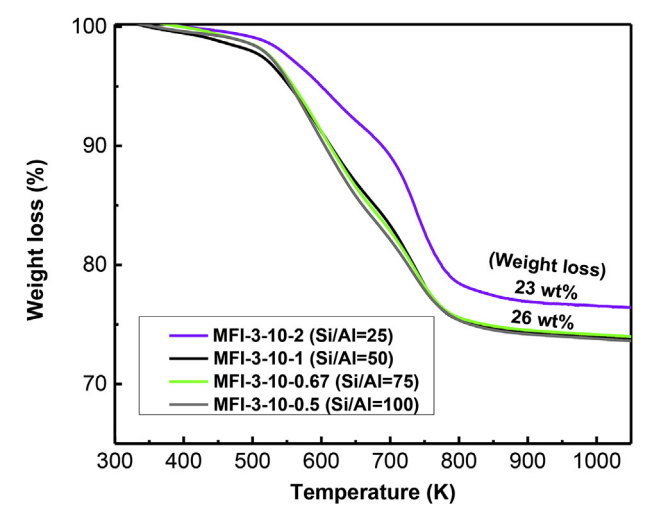


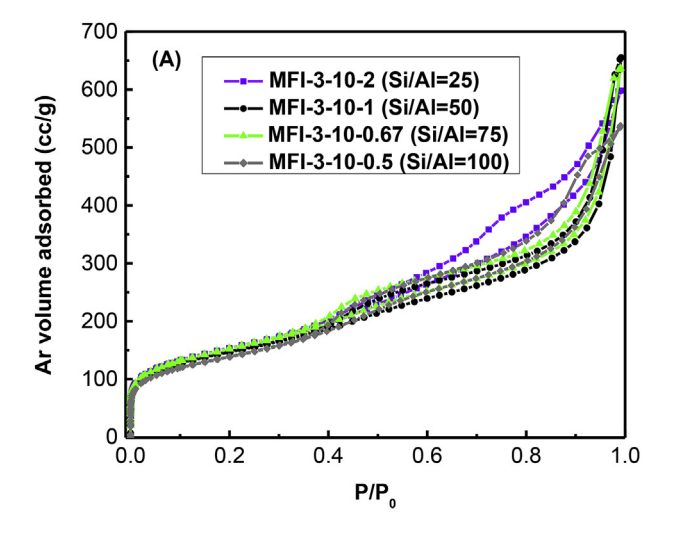
Fig. 12. TGA curves for the synthesized MFI-3-10-2 (Si/Al = 25), MFI-3-10-1 (Si/Al = 50), MFI-3-10-0.67 (Si/Al = 75), and MFI-3-10-0.5 (Si/Al = 100) zeolite samples, respectively.

shown for MFI-3-5-0.5, MFI-3-10-0.5, MFI-3-15-0.5, and MFI-3-18.5-0.5 samples, the crystalline MFI structure was formed indicated by appearance of the MFI zeolite characteristic diffraction peaks. The lowangle XRD reflection peaks ($2\theta = \sim 1.54^\circ$ and 4.02°) in Fig. 5(A) are relatively weak in all cases, demonstrating that the alkalinity of the zeolite synthesis gel is not responsible for the long range ordering of the zeolite nanosheets. Instead, the concentration of $C_{22\text{-}6\text{-}6}$ is primarily responsible for the nanosheet ordering, as indicated by the XRD data in Fig. 1(A). The removal of surfactant template by calcination apparently deteriorated the nanosheet ordering since the low-angle XRD diffraction peaks were completely disappeared in Fig. 5(B).

SEM images of the synthesized hierarchical lamellar MFI zeolites presented in Fig. 6 demonstrate that the amorphous particles exist in MFI-3-0.5-0.5 sample (Fig. 6(A)), while all the other three samples

(Fig. 6(B)-6(D)) have crystallized plate-like particle aggregates. The zeolite nanosheets were not formed in MFI-3-0.5-0.5 due to the insufficient basicity of the zeolite synthesis gel that might not be able to dissolve the silica and alumina materials to form nutrients for zeolite nanosheet growth. By increasing the sodium hydroxide concentration, lamellar MFI structure was formed with randomly organized plate-like nanosheet stacks (MFI-3-5-0.5 in Fig. 6(B)) and intergrown nanosheet aggregates (MFI-3-10-0.5 and MFI-3-15-0.5 in Fig. 6(C) and 6(D), respectively). TEM data shown in Fig. 7 were used to further understand the intergrowth phenomena in the MFI-3-5-0.5, MFI-3-10-0.5, and MFI-3-15-0.5 zeolite samples. As shown in Fig. 7(A)1-3, the MFI-3-5-0.5 sample has some intergrowth from the main body of rod-like zeolite structure. The hierarchical MFI product is analogous to the shape of "plane" or "dragonfly", in which the wings were formed from the intergrowth. The increase in alkalinity of the synthetic gel resulted in more pronounced intergrowth. Fig. 7(B)1-3 indicates the multiple wings formed in the main body of "plane" or "dragonfly" for MFI-3-10-0.5 sample. The further increase in alkalinity enhanced the intergrowth significantly since all the wings of "plane" or "dragonfly" particles seemed to grow into a web, as shown by the MFI-3-15-0.5 sample in Fig. 7(C)1-3. It is reported that Na⁺ ions could template sequential growth from zeolite nanosheets that are directed by the surfactant molecules [29]. The effects of alkalinity on intergrowth of zeolite has been reported by Okubo and co-workers previously [45]. The promotion of intergrowth from zeolite nanosheets with increasing alkalinity in the present study should be due to the combination of Na+ ion templating effect and increased solubility of zeolite nutrient materials.

Fig. 8 shows the TGA measurement results for MFI-3-y-0.5 zeolite samples synthesized under different alkalinity levels of the synthesis gel. The weight loss of the MFI-3-0.5-0.5 zeolite sample due to removal of C_{22-6-6} by calcination is very low (8 wt%), which is consistent with formation of amorphous zeolite particles, as confirmed by the XRD and SEM results. The increase in Na₂O concentration from 5 to 18.5 for MFI-3-5-0.5 to MFI-3-18.5-0.5 increased C_{22-6-6} content in the final hierarchical lamellar MFI products. The weight losses of the samples MFI-3-5-0.5, MFI-3-10-0.5, MFI-3-15-0.5, and MFI-3-18.5-0.5 were 24 wt%,



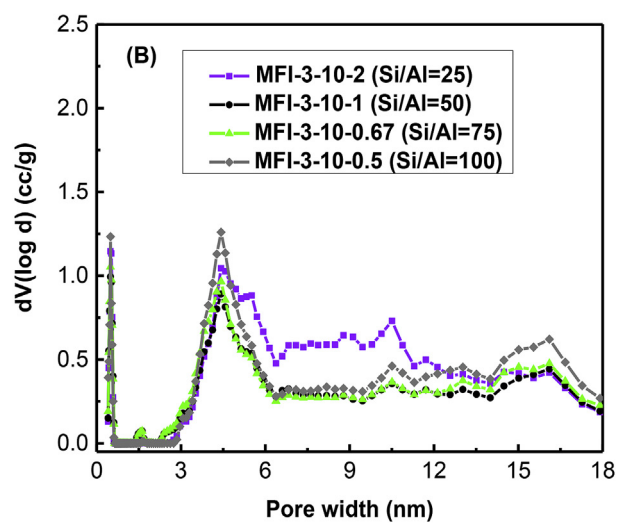


Fig. 13. Ar adsorption-desorption isotherms (A) and NLDFT pore size distribution (B) extracted from adsorption branch of the Ar isotherms for the synthesized MFI-3-10-2 (Si/Al = 25), MFI-3-10-1 (Si/Al = 50), MFI-3-10-0.67 (Si/Al = 75), and MFI-3-10-0.5 (Si/Al = 100) zeolite samples, respectively.

26 wt%, 28 wt%, and 31 wt%, respectively. These results indicate that alkalinity of the zeolite synthesis gel promotes the involvement of C_{22-6-6} template in the hydrothermal crystallization process.

Textural properties of the MFI-3-5-0.5, MFI-3-10-0.5, MFI-3-15-0.5, and MFI-3-18.5-0.5 zeolites were investigated by the Ar adsorption-desorption measurements. Fig. 9 shows the Ar isotherms and the corresponding NLDFT pore size distributions that were derived from the adsorption branches of the Ar isotherms for these samples. All of these hierarchical lamellar MFI zeolites exhibited type IV Ar sorption isotherms (Fig. 9(A)), showing a capillary condensation around the

relative pressure range, $P/P_0 = 0.4$ –0.9 [25]. The H4 shape of the hysteresis loops confirms the presence of narrow slit-shaped pores in these samples, as confirmed in Fig. 9(B). The average mesopore size slightly increases from 4.1 nm to 5 nm for MFI-3-5-0.5 to MFI-3-18.5-0.5 by increasing the NaOH concentration in the synthesis gel. Higher mesopore peak intensity, however, is observed for MFI-3-10-0.5 and MFI-3-15-0.5 samples prepared under medium levels of Na₂O concentration (y = 10 and 15) compared to MFI-3-5-0.5 and MFI-3-18.5-0.5 zeolites. This means that there is an optimal alkalinity level needed for production of hierarchical lamellar MFI structures with maximum mesoporosity. Control MFI shows the lowest mesopore intensity compared to all the other synthesized hierarchical lamellar MFI samples.

Textural properties of these samples were extracted from the Ar isotherms and are shown in Table 3. It should be noted that the $V_{\rm meso}$, $S_{\rm ext}$, $S_{\rm BeT}$, and $V_{\rm t}$ of the MFI-3-10-0.5 and MFI-3-15-0.5 samples synthesized by medium levels of Na_2O concentration are higher than those for MFI-3-18.5-0.5 and control MFI, while their micropore surface areas $(S_{\rm micro})$ and volumes $(V_{\rm micro})$ are comparable. These results illustrate that a medium level of alkalinity of the zeolite synthesis solution is needed to balance the intergrowth to form pillars and thus higher mesoporosity and structure hierarchy. The low level of NaOH content was not enough the drive zeolite nanosheet crystallization and zeolite intergrowth. The high level of alkalinity led to a pronounced sequential growth that spanned the mesoporous areas in the hierarchical lamellar zeolite structure. The optimal NaOH quantity could balance the crystallization of zeolite nanosheets and sequential growth that functions as sparsely distributed pillars to create mesoporosity in the final products.

3.3. Effect of Si/Al ratio on synthesis of hierarchical lamellar MFI zeolite

In order to examine the effect of Si/Al ratio in the zeolite synthesis gel on the resultant hierarchical lamellar MFI zeolites, MFI-3-10-z samples with $z=0.5,\ 0.67,\ 1$, and 2 were synthesized, respectively, which corresponds to Si/Al ratio of 100, 75, 50, and 25 in sequence (Table 1). Fig. 10(A) and 10(B) show the XRD patterns of the MFI-3-10-z zeolites before and after the template removal by calcination, respectively. The wide-angle XRD reflection peaks ($2\theta > 7^\circ$) observed for all of these zeolite samples confirm their crystalline MFI structure, while the presence of low-angle XRD peaks ($2\theta = \sim 1.49^\circ$ and 3.98°) for MFI-3-10-1.0, MFI-3-10-0.67, and MFI-3-10-0.5 shows that the long range structural order of these samples was present, in comparison with MFI-3-10-2.0 sample. After calcination, as it can be seen in Fig. 10(B), all the zeolite structures preserve their crystallinity, but the ordering of the nanosheets was absent, as indicated by the absence of low-angle XRD peaks.

SEM images of these samples are shown in Fig. 11, illustrating that the length of the MFI zeolite nanosheets increases by decreasing the Al content in the zeolite synthesis recipe for MFI-3-10-2.0 with Si/Al ratio of 25 to MFI-3-10-0.5 with Si/Al ratio of 100, in sequence. This phenomenon can be due to the presence of Al in the synthesis recipe which can limit the growth of the MFI nanosheets in a-c directions [12]. TGA analysis of the MFI-3-10-0.5, MFI-3-10-0.67, MFI-3-10-1.0, and MFI-3-10-2.0 shown in Fig. 12 demonstrates that the incorporation of C_{22-6-6}

Table 4Textural properties of the MFI-3-10-z samples determined from Ar isotherms.

V _{meso} [cm ³ g ¹]	$S_{BET}^{d} [m^2 g^{-1}]$
0.693	500
0.722	499
0.733	519
0.644	458
	0.693 0.722 0.733

^a Determined from t-plot method.

^b Determined by NLDFT method.

^c Determined from $V_{meso} = V_t - V_{micro}$.

^d Determined from Brunauer, Emmett, and Teller (BET) method.

Table 5
Comparison of the Si/Al ratios, acid site accessibility, and concentration of Brønsted acid sites for the synthesized hierarchical lamellar MFI zeolite samples.

Zeolite sample	Si/Ala	Si/Al ^b	Concentration of Al sites c (mmol g $^{-1}$)	Concentration of Brønsted acid sites $^{\rm d}$ (mmol g $^{-1}$)	Acid site accessibility ^e (%)
MFI-1-18.5-0.5	100	72	0.228	0.188	10
MFI-3-18.5-0.5	100	63	0.260	0.223	18
MFI-5-18.5-0.5	100	95	0.174	0.164	22
MFI-7-18.5-0.5	100	74	0.222	0.199	21
MFI-3-15-0.5	100	90	0.183	0.195	_
MFI-3-10-0.5	100	99	0.167	0.170	_
MFI-3-5-0.5	100	96	0.172	0.144	_
MFI-3-0.5-0.5	100	129	0.128	0.001	_
MFI-3-10-0.67	75	76	0.216	0.197	_
MFI-3-10-1.0	50	47	0.347	0.291	_
MFI-3-10-2.0	25	25	0.641	0.304	_
Control MFI	50	46	0.355	0.342	12

- ^a Theoretical ratio determined from the zeolite synthesis recipe.
- ^b Determined from ICP-OES method.
- ^c Calculated from Si/Al ratio determined by ICP-OES method.
- ^d Determined using RGC method.
- ^e Determined by DTBP titration in the methanol dehydration reaction experiment.

to the hierarchical lamellar MFI zeolite structure did not significantly depend on the Al content in its structure since the weight loss of all these samples are very similar in the range of 23-26 wt%. The effect of Si/Al ratio in the zeolite synthesis recipe on textural properties of the resulting samples was further studied by means of Ar adsorption-desorption measurements and the results have been shown in Fig. 13. All the synthesized MFI-3-10-z samples at different Si/Al ratios show type IV isotherms with the hysteresis loops related to mesoporous materials (as shown in Fig. 13(A)), MFI-3-10-2.0 sample with lowest Si/Al ratio (Si/Al = 25) displays type H3 hysteresis corresponding to slit-shaped pores while MFI-3-10-1.0, MFI-3-10-0.67, and MFI-3-10-0.5 zeolites (Si/Al = 50, 75, and 100, respectively) have type H4 hysteresis correlated to narrower slit-shaped pores. The NLDFT pore size distribution of these samples in Fig. 13(B) also confirms the presence of more uniform mesopores with average size of $\sim 4.5 \, \text{nm}$ in these three samples. Textural properties of these MFI-3-10-z samples synthesized using different molar ratios of Si/Al in the recipe extracted from Ar sorption measurements have been summarized in Table 4. It can be seen that all these multi-lamellar MFI zeolites have similar mesoporous and microporous textural properties even though their morphology (as shown in Fig. 11) was slightly different from each other due to the different size of the nanosheets in these samples. Therefore, it can be concluded that the Si/Al ratio of the zeolite synthesis gel does not significantly affect the textural properties of the resulting multi-lamellar MFI zeolite.

3.4. Acidity analysis in synthesized hierarchical lamellar MFI zeolites

The Si and Al concentrations of the synthesized hierarchical lamellar MFI zeolites were measured by ICP-OES technique. The concentration of Brønsted acid sites was determined by RGC method. The fraction of external Brønsted acid sites, i.e., accessibility of external Brønsted acid sites to bulky molecules, was quantified by the rate loss in methanol dehydration reaction in the presence of DTBP titrants. Table 5 summarizes all these acidity measurement results. For the synthesized MFI-x-18.5-0.5 zeolites, which had the C_{22-6-6} concentration (x = 1, 3,5, and 7) variation in the synthesis recipe, the Si/Al ratio of the final products are slightly lower than the theoretical Si/Al ratio of 100. For MFI-3-y-0.5 zeolite samples synthesized at different alkalinity levels (y = 5, 10, and 15) of the zeolite synthesis gel, the actual Si/Al ratios in the products are quite close to the theoretical Si/Al ratio of 100 based on the synthesis recipe of these zeolites. For the synthesized MFI-3-10-z zeolites using different amount of aluminum (z) in the synthesis recipe, the Si/Al ratios in the final products are also similar to the theoretical Si/Al ratio in the synthesis recipe (z = 25, 50, 75,and 100). These results suggest that the surfactant template concentration influences the incorporation of the silica and/or alumina nutrients into the final product, while the alkalinity and Si/Al ratio did not affect the final products significantly. The match between the template concentration and alkalinity is needed to achieve successful incorporation of the Si and Al used in the zeolite synthesis gel into the framework structure of the synthesized samples.

The concentration of Brønsted acid sites in each sample was determined and compared to the concentration of Al sites. For most of the synthesized samples, the number of Brønsted acid sites is comparable to that of the Al sites in each sample, suggesting that the Al was incorporated into the zeolite framework successfully. When the Si/Al ratio in the synthetic gel was low, the incorporated Al sites in the framework were low, as indicated by the samples MFI-3-10-1.0 and MFI-3-10-2.0. The amorphous MFI-3-0.5-0.5 did not have any Brønsted acid sites, which is consistent with its amorphous structure. The accessibility of the synthesized MFI-1-18.5-0.5, MFI-3-18.5-0.5, MFI-5-18.5-0.5, and MFI-7-18.5-0.5 zeolite samples to DTBP molecules was 10, 18, 22, and 21, respectively, which is higher than 12 measured for control MFI. This increasing trend is consistent with the increase in mesoporosity of these materials. By simply tuning the composition of the synthesis recipe, we can achieve the tailored intergrowth in the hierarchical lamellar MFI zeolites, which determines their mesoporosity and acid sites accessibility.

4. Conclusions

In summary, the hierarchical lamellar MFI zeolites were synthesized by using a composition of $100SiO_2/1Al_2O_3/3C_{22-6-6}/10Na_2O/4000H_2O$. In comparison to the multi-lamellar MFI prepared using a molar com $position \quad of \quad 100 SiO_2/1 Al_2O_3/10C_{22-6-6}/30 Na_2O/18H_2SO_4/4000H_2O,$ the present recipe eliminated the sodium sulfate and reduced the usage of surfactant templates. The effects of C₂₂₋₆₋₆ content, alkalinity tuned by NaOH amount, and Si/Al ratio on the structural and textural properties of the resultant hierarchical lamellar MFI zeolites were investigated. The results showed that the mesoporosity in the products increases with increasing C_{22-6-6} content, increases and then decreases with increasing NaOH concentration, and is kept nearly constant with changing the Si/Al ratio in the synthesis recipe. The change in mesoporosity of these synthesized samples can be explained by the difference in intergrowth between MFI zeolite nanosheets observed under SEM and TEM, which is governed by the cooperative and sequential templating effects of Na⁺ and C₂₂₋₆₋₆ contents. The acid sites accessibility in the resultant hierarchical lamellar MFI zeolites is consistent with their mesoporosity features. Therefore, the present work demonstrates a simple and cost-effective route for production of hierarchical

meso-/microporous lamellar zeolite with structure hierarchy and acid site accessibility that can be tailored easily by composition variation in the synthetic gel.

Acknowledgements

The authors gratefully acknowledge financial support from National Science Foundation (NSF-CBET1705284, 1642405, 1264599 and 1351384). We acknowledge the support of Maryland NanoCenter and its AIMLab. The AIMLab is supported in part by the NSF as a MRSEC Shared Experimental Facility. This material is based upon work supported by, or in part by, the U.S. Army Research Laboratory and the U.S. Army Research Office under contract/grant number: W911NF-17-1-0363.

References

- [1] A. Corma, Chem. Rev. 97 (1997) 2373.
- [2] A. Corma, J. Catal. 216 (2003) 298.
- [3] C.S. Cundy, P.A. Cox, Chem. Rev. 103 (2003) 663.
- [4] G. Bellussi, A. Carati, C. Rizzo, R. Millini, Catal. Sci. Technol. 3 (2013) 833.
- [5] J. Čejka, G. Centi, J. Perez-Pariente, W.J. Roth, Catal. Today 179 (2012) 2.
- [6] A. Corma, Chem. Rev. 95 (1995) 559.
- [7] J. Čejka, S. Mintova, Catal. Rev. 49 (2007) 457.
- [8] M.E. Davis, Nature 417 (2002) 813.
- [9] M. Choi, H.S. Cho, R. Srivastava, C. Venkatesan, D.H. Choi, R. Ryoo, Nat. Mater. 5 (2006) 718.
- [10] J.C. Groen, J.A. Moulijn, J. Perez-Ramirez, J. Mater. Chem. 16 (2006) 2121.
- [11] C. Jo, K. Cho, J. Kim, R. Ryoo, Chem. Commun. (J. Chem. Soc. Sect. D) 50 (2014)
- [12] K. Na, M. Choi, W. Park, Y. Sakamoto, O. Terasaki, R. Ryoo, J. Am. Chem. Soc. 132 (2010) 4169.
- [13] J. Cejka, G. Centi, J. Perez-Pariente, W.J. Roth, Catal. Today 179 (2012) 2.
- [14] Y. Tao, H. Kanoh, L. Abrams, K. Kaneko, Chem. Rev. 106 (2006) 896.
- [15] E. Verheyen, C. Jo, M. Kurttepeli, G. Vanbutsele, E. Gobechiya, T.I. Korányi, S. Bals, G. Van Tendeloo, R. Ryoo, C.E.A. Kirschhock, J.A. Martens, J. Catal. 300 (2013) 70.
- [16] K. Moller, T. Bein, Chem. Soc. Rev. 42 (2013) 3689.
- [17] D.P. Serrano, J.M. Escola, P. Pizarro, Chem. Soc. Rev. 42 (2013) 4004.
- [18] L.-H. Chen, X.-Y. Li, J.C. Rooke, Y.-H. Zhang, X.-Y. Yang, Y. Tang, F.-S. Xiao, B.-L. Su, J. Mater. Chem. 22 (2012) 17381.

- [19] W. Fan, M.A. Snyder, S. Kumar, P.S. Lee, W.C. Yoo, A.V. McCormick, R.L. Penn, A. Stein, M. Tsapatsis, Nat. Mater. 7 (2008) 984.
- [20] C.J.H. Jacobsen, C. Madsen, J. Houzvicka, I. Schmidt, A. Carlsson, J. Am. Chem. Soc. 122 (2000) 7116.
- [21] J.C. Groen, T. Bach, U. Ziese, A. Donk, K.P. de Jong, J.A. Moulijn, J. Perez-Ramirez, J. Am. Chem. Soc. 127 (2005) 10792.
- [22] F.J. Liu, T. Willhammar, L. Wang, L.F. Zhu, Q. Sun, X.J. Meng, W. Carrillo-Cabrera, X.D. Zou, F.S. Xiao, J. Am. Chem. Soc. 134 (2012) 4557.
- [23] M. Tsapatsis, AIChE J. 60 (2014) 2374.
- [24] K. Na, W. Park, Y. Seo, R. Ryoo, Chem. Mater. 23 (2011) 1273.
- [25] M. Choi, K. Na, J. Kim, Y. Sakamoto, O. Terasaki, R. Ryoo, Nature 461 (2009) 246.
- [26] J. Jung, C. Jo, K. Cho, R. Ryoo, J. Mater. Chem. 22 (2012) 4637.
- [27] W. Park, D. Yu, K. Na, K.E. Jelfs, B. Slater, Y. Sakamoto, R. Ryoo, Chem. Mater. 23 (2011) 5131.
- [28] C.K. Liu, W. Xu, Microporous Mesoporous Mater. 253 (2017) 160.
- [29] Y. Kim, K. Kim, R. Ryoo, Chem. Mater. 29 (2017) 1752.
- [30] A.G. Machoke, I.Y. Knoke, S. Lopez-Orozco, M. Schmiele, T. Selvam, V.R.R. Marthala, E. Spiecker, T. Unruh, M. Hartmann, W. Schwieger, Microporous Mesoporous Mater. 190 (2014) 324.
- [31] D. Liu, A. Bhan, M. Tsapatsis, S. Al Hashimi, ACS Catal. 1 (2011) 7.
- [32] L. Emdadi, Y. Wu, G. Zhu, C.-C. Chang, W. Fan, T. Pham, R.F. Lobo, D. Liu, Chem. Mater. 26 (2014) 1345.
- [33] O.A. Abdelrahman, K.P. Vinter, L. Ren, D. Xu, R.J. Gorte, M. Tsapatsis, P.J. Dauenhauer, Catal. Sci. Technol. 7 (2017) 3831.
- [34] L. Emdadi, S.C. Oh, Y. Wu, S.N. Oliaee, Y. Diao, G. Zhu, D. Liu, J. Catal. 335 (2016) 165.
- [35] Y. Wu, L. Emdadi, S.C. Oh, M. Sakbodin, D. Liu, J. Catal. 323 (2015) 100.
- [36] Y. Wu, Z. Lu, L. Emdadi, S.C. Oh, J. Wang, Y. Lei, H. Chen, D.T. Tran, I.C. Lee, D. Liu, J. Catal. 337 (2016) 177.
- [37] B. Liu, C. Wattanaprayoon, S.C. Oh, L. Emdadi, D. Liu, Chem. Mater. 27 (2015) 1479.
- [38] K.S.W. Sing, D.H. Everett, R.A.W. Haul, L. Moscou, R.A. Pierotti, J. Roquerol, T. Siemieniewska, Pure Appl. Chem. 57 (1985) 603.
- [39] M. Thommes, Textural charaterization of zeolite and ordered mesoporous materials by physical adsoption, in: J. Cejka, H. van Bekkum, A. Corma, F. Schüth (Eds.), Introduction to Zeolite Science and Practice, 3rd revised Edition, Elsevier, 2007, p. 495
- [40] M. Milina, S. Mitchell, N.-L. Michels, J. Kenvin, J. Pérez-Ramírez, J. Catal. 308 (2013) 398.
- [41] M. Thommes, S. Mitchell, J. Pérez-Ramírez, J. Phys. Chem. C 116 (2012) 18816.
- [42] J.D. Epping, B.F. Chmelka, Curr. Opin. Colloid Interface Sci. 11 (2006) 81.
- [43] H. Lechert, Microporous Mesoporous Mater. 22 (1998) 519.
- [44] H.-S. Oh, K.-K. Kang, M.-H. Kim, H.-K. Rhee, Kor. J. Chem. Eng. 18 (2001) 113.
- [45] S.H. Keoh, W. Chaikittisilp, K. Muraoka, R.R. Mukti, A. Shimojima, P. Kumar, M. Tsapatsis, T. Okubo, Chem. Mater. 28 (2016) 8997.